Nanoscale

Accepted Manuscript

This article can be cited before page numbers have been issued, to do this please use: K. Zhao, R. Peng and D. Li, *Nanoscale*, 2016, DOI: 10.1039/C6NR06952E.

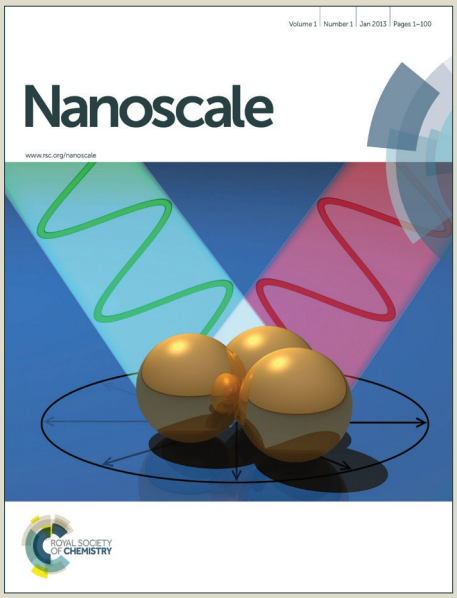

View Article Online
DOI: 10.1039/C6NR06952E

Journal Name

ARTICLE

Separation of nanoparticles by a nano-orifice based DC-Dielectrophoresis method in pressure-driven flow

Received 00th January 20xx,
Accepted 00th January 20xx

DOI: 10.1039/x0xx00000x

www.rsc.org/

Kai Zhao[a], Ran Peng[a] and Dongqing Li*[a]

A novel DC-Dielectrophoresis (DEP) method employing pressure-driven flow for the continuous separation of micro/nano-particles is presented in this paper. To generate the DEP force, a small voltage difference is applied to produce the non-uniformity of the electric field across a microchannel via a larger orifice of several hundred microns on one side of the channel wall and a smaller orifice of several hundred nanometers on the opposite channel wall. The particles experience DEP force when they move with the flow through the vicinity of the small orifice, where exits the strongest electrical field gradient. Experiments were conducted to demonstrate the separation of 1 μm and 3 μm polystyrene particles by size by adjusting the applied electrical potentials. In order to separate smaller nanoparticles, the electrical conductivity of the suspending solution is adjusted so that the polystyrene nanoparticles of a given size experience positive DEP while the polystyrene nanoparticles of another size experience negative DEP. Using this method, the separation of 51 nm and 140 nm nanoparticles and the separation of 140 nm and 500 nm nanoparticles were demonstrated. In comparison with the microfluidic DC-DEP methods reported in the literatures which utilize hurdles or obstacles to induce the non-uniformity of electric field, a pair of asymmetrical orifices on the channel side walls is used in this method to generate strong electrical field gradient and has advantages such as capability of separating nanoparticles, and locally applied lower electrical voltages to minimize Joule heating effect.

Introduction

The rapid development of micro total analysis systems (μTAS) and lab-on-a-chip (LOC) devices has attracted growing interest in recent decades [1–3]. LOC systems bring miniaturization, parallelization, and integration to the analyses and applications in chemical, biological and clinical fields [4–6]. One of the crucial applications is the continuous and accurate manipulation of microparticles and nanoparticles [7–15], such as bacteria [16–18], protein [19–21], DNA [22], virus [23–25] and cells [26–28]. Among the various technologies that have been developed and utilized to manipulate particles in microfluidic systems, such as mechanical, optical, magnetic, thermal, chemical, acoustic and electrical methods [29–38], dielectrophoresis (DEP) may be the most popular method because it is label-free, scalable, and capable of generating both negative and positive forces to manipulate bio-particles [28,39].

DEP is the motion of a dielectric particle in an aqueous solution due to the polarization effects in a non-uniform electric field. Traditionally, the non-uniform electric field is induced by applying an alternate current (AC) electric field across arrays of micron structured electrodes of various shapes and configurations [11,40]. Rajaram et al. [13] demonstrated the manipulation of nanoparticles derivatized by DNA with arrays of microelectrodes which are coated with the layers of the porous hydrogel in an AC electric field. Gascoyne et al. [41] investigated that the positive DEP force created by arrays of castellated microelectrodes can be used for the separation of the mammalian cell under AC electric field conditions. Khashayar et al. [42] established an optical waveguide by concentration 250 nm particles made of silica by DEP in AC electric fields. Yu et al. [43] designed an array of 3-D elliptic electrodes in a microchannel for the focusing of human leukemia HL60 cells to the middle of the microchannel from all directions. Generally, the AC electrode-based DEP (eDEP) systems can induce a high gradient of the electric field with low electric voltages. However, it involves issues such as the complexed fabrication of microelectrode, fouling of electrodes [44], and electrochemical reactions on electrode surface [45]. These shortcomings are overcome in the insulator-based DEP (iDEP) systems, where direct current (DC) electric field is applied via two external electrodes over an array of specifically patterned structures, such as insulator obstacles or hurdles inside microchannels, to generate the non-uniform electric field. Because of using DC electric field, the iDEP is also considered as DC-DEP. Cummings and Singh [46] showed the trapping of 200 nm polystyrene particles by DEP force with an array of insulator rods inside the microchannel. Lapizco-Encinas et al. [16,47] investigated the manipulation and separation of bacterial of live/dead E.coli, and the

[a] Department of Mechanical and Mechatronics Engineering, University of Waterloo, Waterloo, Ontario, Canada, N2L 3G1. E-mail: dongqing@uwaterloo.ca
†Electronic Supplementary Information (ESI) available: [details of any supplementary information available should be included here]. See DOI: 10.1039/x0xx00000x

View Article Online
DOI: 10.1039/C6NR06952E

manipulation and selective separation of two types of live bacterial with arrays of circular insulator posts inside microchannel in DC electric fields. Kang et al. [9,26] demonstrated the separation of polystyrene particles by size with an insulator hurdle in the microchannel in DC electric fields. Chen [12] investigated a rapid concentration of 500 nm to 1 μm nanoparticles with an insulator 'tree' structure under DC electric fields in the microchannel. Generally, the DC-DEP chips are simple to be fabricated, and mechanically robust and chemically inert [26]. However, high voltages are typically required for DC-DEP to induce sufficiently strong DEP forces. The high voltages applied through the whole microchannel (end to end) may induce Joule heating inside the microchannel. This effect may limit their applications to manipulate biological particles and decrease the performance of the microfluidic chips [48]. The viability of cells can be affected by varying temperature inside the microchannel, and 4℃ temperature increase above the cell physiological temperature can lead to cell death [28]. Furthermore, due to the limitation of the microfabrication techniques, the smallest space formed by the insulator hurdles/obstacles in the microchannel is relatively large, typically tens of microns. Consequently, the resulting gradient of the non-uniform electric field is not sufficiently high. This is a key reason that the existing DC-DEP methods cannot be used for the separation of nanoparticles by size.

In this paper, a novel microfluidic chip using a pair of asymmetrical orifices to generate a locally strong electric field gradient is proposed. By applying DC electric fields via a small orifice and a large orifice on the opposite sides of channel walls to induce the spatial non-uniform electric field, the aforementioned adverse effects such as the complicated process of embedding microelectrodes, the electrode fouling, and electrode surface reactions are avoided. Moreover, by using the pressure-driven flow in the microchannel to transport particles and applying low electric voltages locally, the undesirable effects of the electric fields, such as Joule heating, have been significantly reduced. Choosing an appropriate size ratio of the small orifice and the large orifice enables the generation of sufficiently large electric field gradient and hence sufficiently large DEP forces, therefore, the separation of microparticles with smaller size differences and separation of nanoparticles are possible. In this paper, theoretical analysis on the generation of the non-uniform electric field around the small orifice is conducted. Then, the successful experimental separation of 1 μm and 3 μm polystyrene particles by adjusting the applied electrical potentials are presented and discussed. Furthermore, the effects of the structure of the small orifice and the pressure-driven flow on the DC-DEP separation are elaborated. Finally, the separation of nanoparticles, 51 nm and 140 nm particles, and 140 nm and 500 nm particles, by adjusting the electrical conductivity of the suspending medium are demonstrated.

Design of the DC-DEP device

To induce the spatially non-uniform electric field, the traditional DC-iDEP method uses insulator obstacles or hurdles inside the microchannel, as illustrated in Figure 1a [39]. The DC electric field in the microchannel is applied by the two electrodes inserting in the inlet and exit reservoirs, respectively. The flow is also induced by the applied DC electric field, i.e., electroosmotic flow (EOF). The general expression for the DEP force exerted on a spherical particle is expressed as [49]

$$\mathrm{F_{DEP}} = 2\pi\varepsilon_m\, r^3\, \mathrm{Re}(f_{\mathrm{CM}})(\nabla|E|^2) \qquad \text{Eq. (1)}$$

where ε_m is the electrical permittivity of the suspending solution, r is the radius of particle, $\nabla|E|^2$ is the gradient of electric field square and $\mathrm{Re}(f_{\mathrm{CM}})$ is the real part of Clausius-Mossotti (CM) factor which is given by

$$\mathrm{f_{CM}} = \left(\frac{\varepsilon_{\mathrm{p}}^* - \varepsilon_{\mathrm{m}}^*}{\varepsilon_{\mathrm{p}}^* + 2\varepsilon_{\mathrm{m}}^*}\right) \qquad \text{Eq. (2)}$$

where subscripts p and m represent the particle and medium, respectively; $\varepsilon^* = \varepsilon - (j\sigma/\omega)$ is the complex permittivity, σ is the electric conductivity, ω is the angular frequency of the applied electric field, and $j = \sqrt{-1}$. The f_{CM} indicates the relative polarizability of the particles with respect to the surrounding solution. A positive value of CM factor indicates that the particle will experience a positive DEP (i.e., moving towards the strong electric fields), while a negative value of CM factor demonstrates that the particle will experience a negative DEP (i.e., moving towards the weak electric fields).

It can be seen from Eq (1) that the value of the DEP force is proportional to the gradient of electric field square ($\nabla|E|^2$) and the particle size (r^3). As the trajectory shift of the particles is proportional to the value of the DEP force exerting on the

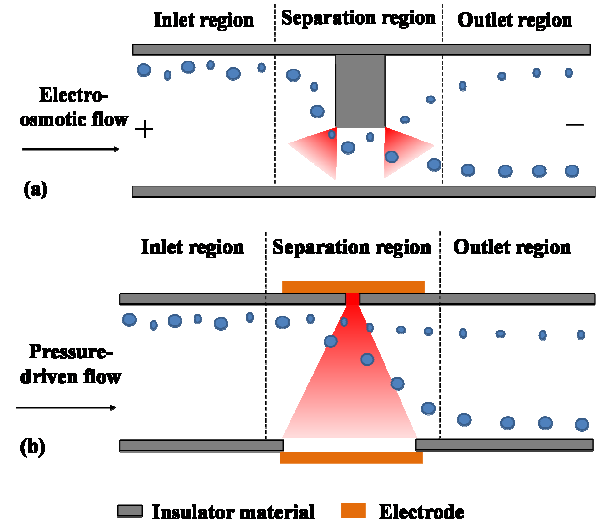

Figure 1. Schematic illustration of DC-DEP microfluidic channel: (a) In the traditional DC-iDEP method, the non-uniform electric field is induced by an insulator hurdle. (b) In the new orifice-based DC-DEP method, the non-uniform electric field is created by using the asymmetric orifices on opposite channel walls (red colour represents the electric field strength).

View Article Online
DOI: 10.1039/C6NR06952E

particles, the particles with different sizes will be separated and moved into different streams after passing over the non-uniform electric field region. However, in order to separate particles of smaller sizes and particles with small size differences, a strong DEP force is necessary, which means a high electric field gradient near the hurdle is required. To achieve high ($\nabla|E|^2$), one way is to apply a higher voltage difference along the entire channel (Figure 1a) which may cause unwanted side effects such as the Joule heating as mentioned above. Another way is to make the gap between the tip of the hurdle and the channel wall very small. However, conventional microfabrication methods (e.g., soft lithography) generally cannot make the gap smaller than 10 μm. In addition, when the gap is sufficiently small, polarized particles may form clusters near the gap and block the gap, preventing the particles from passing through the gap.

To solve the above-mentioned problems in the traditional DC-iDEP method, a novel orifice based DC-DEP method employing pressure-driven flow is proposed, as illustrated in Figure 1b. The non-uniform electric field is induced by applying DC electric fields across the channel through a pair of asymmetric orifices: a larger orifice and a small orifice on the opposite sides of channel walls. As shown in Figure 1b, the non-uniformity or the gradient of the electrical field is dependent on the width ratio between the large orifice and the small orifice. A strong non-uniform electrical field can be obtained if the orifices' width ratio is sufficiently large. Since the electric field is applied locally via the orifices across the microchannel, i.e., the distance between the two electrodes is very short, a small voltage difference is sufficient for generating strong electric field; thus Joule heating is essentially avoided. Furthermore, in this design, the generation of the local electrical field gradient does not require changing the cross-section of the microchannel and hence will not impair the transport of the particles. In the traditional DC-iDEP method, the particles move with the electroosmotic flow in the microchannel, and hence the throughput of the particles is very low, typically a few particles per second. In the proposed new method, by using the pressure-driven flow to transport particles, the throughput can be easily increased by ten times or more.

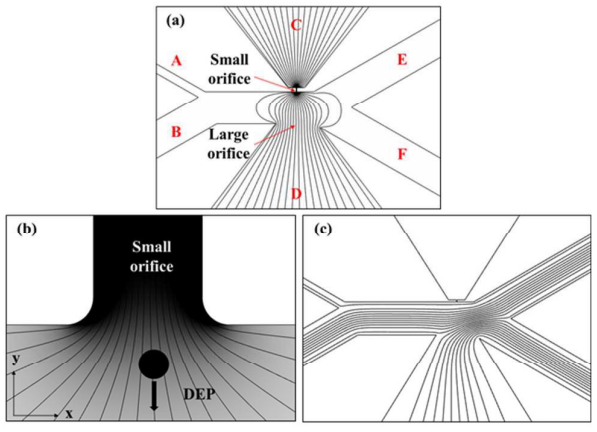

Figure 2. (a) The configuration of the new asymmetric orifice based DC-DEP chip and the distribution of the electric field lines (top view). The stronger electric field is indicated by the darkness. A is the particle inlet channel. B is the focusing flow inlet channel. E and F are the separation outlet channels. C and D are the wells for placing electrodes. (b) An enlarged view of the electric field lines around the small orifice region, and an example of a particle experiencing negative DEP force. (c) Streamlines of the pressure-driven flow field in the microchannel.

The schematic structure of this microfluidic chip from a top view and an example of the distribution of the electric field lines are illustrated in Figure 2a. The entire chip is made of an electrical insulator material such as polydimethylsiloxane (PDMS). The DC electric field is employed through the microchannel by two external electrodes placed in wells C and D, respectively. The non-uniform electric field is generated owing to the asymmetric size of the orifices, a small orifice on one side of the channel walls and a large orifice on the opposite side of the channel walls. The flow field in the microchannel in shown in Figure 2c. Firstly, the particles mixture comes into the main channel as one stream from the inlet channel A, and the particles are forced to move closely to the small orifice by the main stream (focusing flow) of the suspending medium from another inlet channel B. After passing through the vicinity of the small orifice where exits the strongest electrical field gradient, the particles experience DEP force and their trajectories will change. Since the small orifices used in this study are very small, i.e., 510 or 1.5 μm, the fluid flow from channel C to the main channel is negligible. Let us consider particles all experiencing negative DEP force and they will be pushed away towards the weak electric field, i.e., from the small orifice to the large orifice. Since the value of DEP force exerting on particles is proportional to the sizes of the particles, the larger particles will be repelled away further than the smaller particles. Thus, the smaller and the larger particles can move separately into the separation outlet channels E and F, respectively.

To discuss the effects of structure of the orifices on the gradient of electric field square ($\nabla|E|^2$), extensive numerical simulations have been conducted by COMSOL 4.3b. Figure 3 and Table 1 show some examples of the values of $\nabla|E|^2$ obtained for the orifice combinations with two different width ratios, and two different lengths of the small orifice at a given electric potential.

As we know, a higher $\nabla|E|^2$ means a stronger DEP force. It

Table 1. Calculated values of $\nabla|E|^2_{max}$ for different width ratios and different lengths of the small orifice (the width of the large orifice is fixed at 100 μm, the voltage is applied at electrode C while electrode D is grounded, and the distance between the electrodes is 0.15 cm)

Width of the small orifice (μm)	Width ratio	Length of the small orifice (μm)	Applied voltage (V)	$\nabla\|E\|^2_{max}$ (V^2/m^3)
0.5	200	5	100	5.44×10^{21}
1	100	5	100	3.73×10^{21}
1	100	15	100	1.2×10^{21}
1	100	5	150	8.38×10^{21}

View Article Online
DOI: 10.1039/C6NR06952E

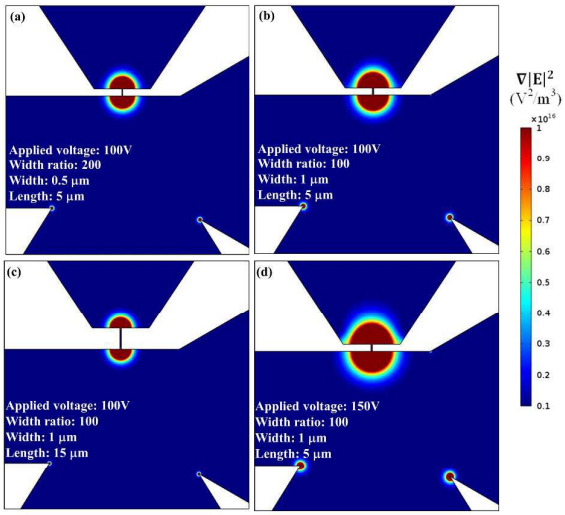

Figure 3. Numerical simulations of the distribution of the gradient of electric field square ($\nabla|E|^2$). (a) Width ratio of the orifices is 200, the width and the length of the small orifice are 0.5 μm and 5 μm, respectively. The applied voltage is 100 V. (b) Width ratio of the orifices is 100, the width and the length of the small orifice are 1 μm and 5 μm, respectively. The applied voltage is 100 V. (c) Width ratio of the orifices is 100, the width and the length of the small orifice are 1 μm and 15 μm, respectively. The applied voltage is 100 V, and (d) Width ratio of the orifices is 100, the width and the length of the small orifice are 1 μm and 5 μm, respectively. The applied voltage is 150 V.

can be inferred from Figure 3a and Figure 3b, the structure with large width ratio produces higher values of $\nabla|E|^2$ (depicted by the darker red color) in the vicinity of the small orifice, but a relatively small region of high $\nabla|E|^2$. For example, the semicircle of the darker red color has a radius of approximately 18 μm in Figure 3a; while the semicircle of the darker red color has a radius of approximately 23 μm in Figure 3b. This is because, when the width of the small orifice is reduced, the electric resistance of the small orifice is increased and hence the electric potential drop inside the small orifice is increased. Thus, the high $\nabla|E|^2$area outside the small orifice becomes smaller under a given applied voltage. Similarly, if the small orifice is long, the electric resistance of the small orifice is large, and hence the electric potential drop inside the small orifice is large. Consequently, the high $\nabla|E|^2$area outside the small orifice is smaller. By comparing Figure 3b and Figure 3c, one can clearly see that the high $\nabla|E|^2$ area is larger in the structure with the shorter small orifice (Figure 3b). Therefore, the structure with relatively large width ratio and a shorter small orifice can lead to large DEP force on the particles, resulting in a high separation resolution. Furthermore, it can be expected that increase of the applied voltage will increase the value of maximum $\nabla|E|^2$ and the high $\nabla|E|^2$ area significantly, as shown in Figure 3d. As seen from Table 1, the value of the $\nabla|E|^2{}_{max}$ increases about 1.5 times when the width ratio increases from 100 to 200, and the value of the $\nabla|E|^2{}_{max}$ increases about 3.1 times when the length of the small orifice is reduced from 15 μm m to 5 μm.

Materials and experimental method

Particles and suspending solution

Polystyrene microspheres (Bangs Laboratory) of three different sizes, 0.5, 1, and 3 μm in diameter were used. In addition, fluorescent polystyrene spheres (Thermo SCIENTIFIC) of two different sizes, 51 nm red (Ex/Em 542/612 nm) and 140 nm green (Ex/Em 468/508 nm) in diameter, were also employed as sample particles. The particles were originally suspended in pure water and further diluted to the concentrations of 3.1×10^9 beads/mL, 3.54×10^8 beads/mL, 3.6×10^7 beads/mL, 2.74×10^{13} beads/mL and 1.32×10^{11}/mL, respectively.

Two suspending solutions were prepared with DI water and K_2HPO_4. A 0.4 mM K_2HPO_4 solution with a pH 7 and an electric conductivity of 1×10^{-2} S/m is used for the separation of 1 μm and 3 μm particles, and the separation of 0.5 μm and 140 nm particles. A 1.6 mM K_2HPO_4 solution with a pH 7 and an electric conductivity of 4×10^{-2} S/m is employed for the separation of 51 nm and 140 nm particles.

Fabrication of microfluidic chips

In this study, in order to generate strong non-uniform electric fields, a small microchannel or a nanochannel is used to form the small orifice on one side of the microchannel walls. The microfluidic chip was made by bonding a top PDMS layer having the microchannel structure (as illustrated in Figure 4g) with a bottom PDMS layer having a single small microchannel or nanochannel. The single small microchannel or nanochannel was obtained by three steps and illustrated in Figure 4(a-f). Firstly, a small micro-crack or nano-crack with a controlled size is generated on a polystyrene surface by the solvent-induced

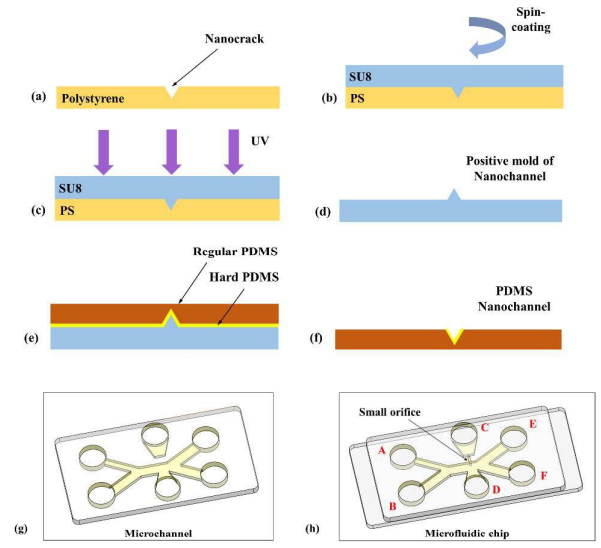

Figure 4. Procedure for the fabrication of the PDMS microfluidic chip with a pair of asymmetric orifices for DC-DEP separation of particles. (a~f) Procedures of making a small microchannel or a nanochannel on a PDMS layer. (g) The top PDMS layer with the microchannel structure. (h) The bonded chip.

View Article Online
DOI: 10.1039/C6NR06952E

method and the detailed fabrication procedure was described elsewhere [50]. Thereafter, the pattern of the negative micro-crack or nano-crack is transferred onto a SU8 photoresist layer (MicroChem Corp.) by the soft lithography technique to work as the positive microchannel or nanochannel mold. Finally, the PDMS microchannel or nanochannel is replicated from the positive mold by casting a 30 μm layer of hard PDMS [51] with a higher Young's modulus and followed by casting a regular PDMS layer of about 2 mm in thickness to avoid the collapse of the small microchannel or nanochannel after the bonding process. The microchannel structure is designed by Auto CAD® software and fabricated by the standard soft photolithography protocol [52]. Finally, the DEP microfluidic chip is obtained by bonding the plasma-treated PDMS layer with the nanochannel (or small microchannel) and the plasma-treated PDMS layer with the microchannels together by using a custom-made alignment system under a microscope (Nikon, TE-2000) as shown in Figure 4(g-h).

A picture of the DC-DEP microfluidic chip is shown in Figure 5. In this study, one nanochannel of 510 nm in width and 450 nm in depth and another small microchannel of 1.5 μm in width and 1.6 μm in depth were fabricated to make the small orifice. Correspondingly, there are two widths of the small orifices used in the experiments, 510 nm and 1.5 μm. For all chips used in this study, the width of the large orifice is always 125 μm. Two lengths of the small orifice, 5 μm and 15 μm, were used for the studies of the effect of small orifice structure on the particles separation. In the chip, as shown in Figure 4h or Figure 5a, there are six channels connected to six different reservoirs. Channel A transports the particle mixture into the main horizontal channel where the particle stream is forced to move close to the wall of the small orifice side by the dominant stream of suspending medium entering from channel B. The main horizontal channel and the branch channels B, E, and F are all 80 μm in width. In order to drive the particles from channel A to move closely to the small orifice, the width ratio between the inlet channels A and B is selected. Two different widths for the inlet channel A were used in this study: 20 μm for the separation of micron size particles, and 10 μm for the separation of nanoparticles. All channels have a depth of 15 μm. The local electric field is induced by the platinum electrodes submerged in wells C and D. The distance between the two external electrodes is approximately 0.4 cm. The separated smaller and larger particles after passing the small orifice region move into the outlet channels E and F, respectively.

Experiment procedures

The DEP particles separation experiments started by filling the microfluidic chip with the suspending medium, at a room temperature of 25±1℃. Next, 10 μL of the particle solution was introduced into the reservoir A, 10 μL of the suspending solution was introduced into the reservoir B, and 5 μL of suspending solution was loaded into the wells C and D for inserting the external electrodes. The liquid flow and the particle transport in the microchannels were all driven by the pressure difference between the inlet and exit wells (i.e., the difference of liquid level). The particles were forced by the main stream flow from channel B to move along the channel wall and pass the vicinity of the small orifice to experience the stronger gradient of the non-uniform electric field. Then the DC power supply (HVS448 High Voltage Sequencer, LabSmith) was utilized to apply DC electric voltages by the external platinum electrodes placed at the reservoirs C and D. The voltage output to the electrodes was adjusted by a home-made voltages controller. In the experiments, the voltage output to electrode C was carefully adjusted to ensure the best particles separation effect and the electrode D is grounded.

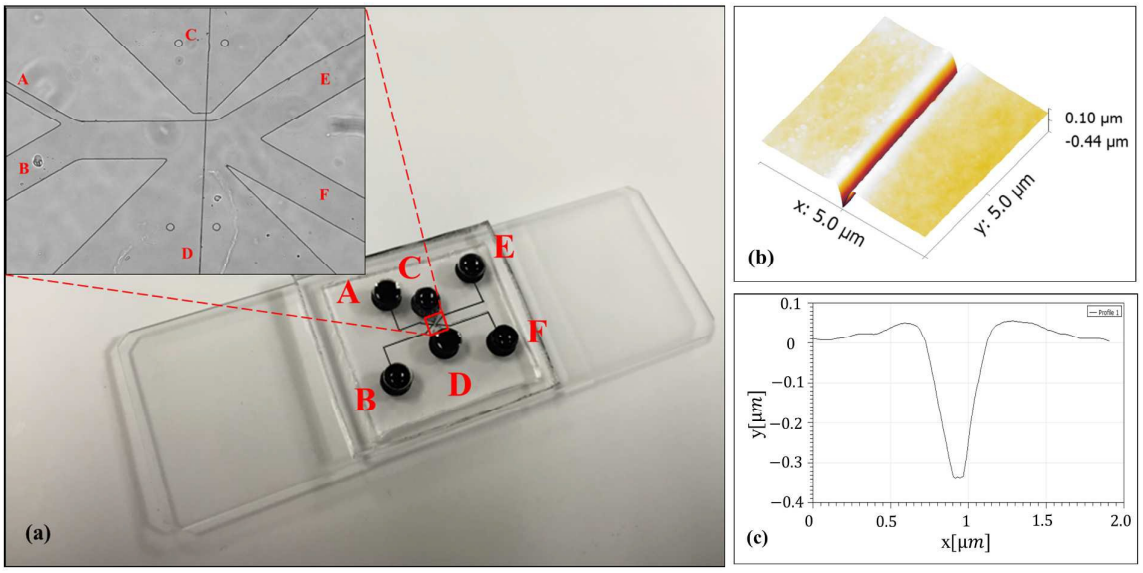

Figure 5. (a) The DC-DEP microfluidic chip made by PDMS. (b) AFM image of the PDMS single nanochannel. (c) Cross section of the PDMS single nanochannel measured by AFM, the width is 510 ± 10 nm and the depth is 450 ± 20 nm.

View Article Online
DOI: 10.1039/C6NR06952E

For the separation of nanoparticles, as the DEP force exerted on nanoparticles is smaller in comparison with that on microparticles, the electrical force (i.e., interaction between the applied electric field and the electrostatic surface charge of the particle) on the particles is adjusted to be in the same direction as the negative DEP force by reversing the polarity of the applied electric field. In this way, the trajectory shifts of the nanoparticles experiencing negative DEP will be enlarged, enhancing the DEP separation. The motion of particles was visualized by an inverted optical microscope (Nikon, TE-2000) and recorded by a digital camera (QImaging) at the frame rate of 25 fps. Under each condition, 3 independent measurements were conducted.

Results and discussion

The DC-iDEP technique can separate particles by size, however, successful separation usually requires the particles to have a large size difference [39]. In the previously reported works of DC-DEP separation by size, the separation of particles cannot be realized for a size difference smaller than 3 μm [9,26,53–56]. However, by using the novel method developed in this work, 1 μm and 3 μm polystyrene particles (with only 2 μm size difference) were successfully separated. Moreover, by adjusting the electric conductivity of the suspending solution, 51 nm and 140 nm particles, and 140 nm and 500 nm particles were also well separated.

Effect of applied voltage on the separation of 1 μm and 3 μm particles

The effect of the applied voltage on the separation of 1 μm and 3 μm particles were conducted by applying different voltages at electrode C from 60 to 160 V. The electrode D is grounded. The 0.4 mM K_2HPO_4 solution with a pH 7 and an electric conductivity of 1×10^{-2} S/m is used as the suspending solution, and the particles experience negative DEP force. In these experiments, the width of the small orifice is 1.5 μm, and the length of the small orifice is 15 μm. The width of the large orifice is 125 μm. The trajectory changes of 1 μm and 3 μm particles under different applied voltages from 60 to 160 V is shown in Figure 6. Each picture was achieved by superimposing series of continuous pictures of the moving particles under a given condition.

It should be realized that according to Eq. (1), the DEP force is proportional to the gradient of electric field square ($\nabla|E|^2$). As the applied voltage increases, the DEP force will increase. Furthermore, it can be seen easily from Eq. (1) that the value of the DEP force exerted on the 3 μm particle is 9 times larger than that on the 1 μm particle. As shown in Figure 6a, under 60 volts, the DEP force is weak, thus there is no apparent trajectory difference between the small particles and the large particles after the particles passed the vicinity of the small orifice. They moved into the outlet channel E. When the applied voltage was increased to 100 volts, as shown in Figure 6b, the larger DEP force made a significant trajectory difference between the small particles and the large particles after the particles passing through the vicinity of the small orifice. However, the trajectory shift of the large particles is not large enough and a significant portion of the large particles was still moved into the outlet channel E with the small particles. As seen in Figure 6c, when increasing the applied voltage to 140 volts, the strong DEP force at the small orifice region caused significant trajectory change for the large particles, so that the 1 μm and 3 μm particles continuously moved into distinct outlet channels E and F. The separation of 1 μm particles and 3 μm particles was achieved. Further increase of the applied voltage can produce an overly strong DEP force and cannot separate the small particles and large particles into the individual outlet channels as desired. For example, under 160 volts, the 3 μm particles were pushed by the DEP force into the reservoir D and the 1 μm particles moved into reservoirs E and F, as shown in Figure 6d.

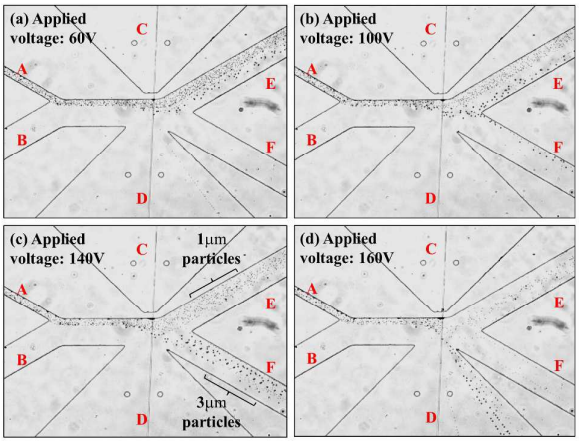

Figure 6. Effect of the applied electric field on the separation of 1 μm and 3 μm particles by the DC-DEP method developed in this work. The dependence of the particles' trajectories on the applied voltage at electrode C (a) 60 V, (b) 100 V, (c) 140 V, and (d) 160 V. The electrode D is grounded.

Effect of pressure-driven flow

To examine the effect of pressure-driven flow, four different volumes inputted into the inlet wells A and B (i.e., four different liquid levels), 10 μL, 12.5 μL, 15 μL, and 17.5 μL, were conducted for the separation of 1 μm and 3 μm particles. Correspondingly, the flow rate is 1.323×10^{-4} μL/s, 1.554×10^{-4} μL/s, 1.692×10^{-4} μL/s, and 1.866×10^{-4} μL/s. In these tests, the electrode C is applied 140 V and the electrode D is grounded. The width and length of the small orifice are 1.5 μm and 15 μm, respectively, and the large orifice width is 125 μm. The trajectory shift of 1 μm and 3 μm particles with different flow rates from 1.323×10^{-4} μL/s to 1.866×10^{-4} μL/s is demonstrated in Figure 7.

Figure 7a illustrates that the 1 μm and 3 μm particles were separated and diverted into different outlet channels at the flow rate of 1.323×10^{-4} μL/s, under 140 volts. It is easy to understand that when the flow rate increases (i.e., the velocity of the particles), the particles move fast and pass over the vicinity of the small orifice. The time period of the particles experiencing the DEP force will decrease. As shown in Figure

View Article Online
DOI: 10.1039/C6NR06952E

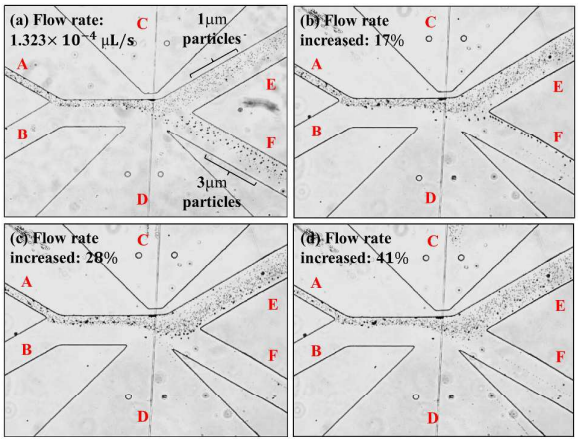

Figure 7. Effect of the flow rate on the separation of 1 μm and 3 μm particles by the DC-DEP method developed in this work. The dependence of the particles' trajectories on pressure-driven flow with flow rate (a) 1.323×10^{-4} μL/s, (b) 1.554×10^{-4} μL/s (17% increase), (c) 1.692×10^{-4} μL/s (28% increase), and (d) 1.866×10^{-4} μL/s (41% increase). The electrode C is applied 140 V and the electrode D is grounded. The width and length of the small orifice are 1.5 μm and 15 μm, respectively, and the large orifice width is 125 μm.

7b, when the flow rate increased by 17% to 1.554×10^{-4} μL/s, the time period of DEP force exerting on the particles is shortened, and the trajectory difference between the small particles and the large particles after passing the vicinity of the small orifice is reduced. Furthermore, the trajectory change of the large particles is not large enough and some of the large particles moved into the outlet channel E with the small particles. When the flow rate increased by 28% to 1.692×10^{-4} μL/s, as shown in Figure 7c, there is no obvious difference of trajectory shift between the small particles and the larger particles after passing the vicinity of the small orifice. The small particles and the larger particles moved into the outlet channel E. Further increase of the flow rate will excessively shorten the action time of the DEP force exerting on the particles, and the small particles and the large particle cannot be separated into the individual outlet channels. As shown in Figure 7d, when the flow rate increased by 41% to 1.866×10^{-4} μL/s, the 1 μm and 3 μm particles were driven into the outlet channel E.

Effect of small orifice structure

As discussed previously, the electric field gradient is strongly depending on the structure of the small orifice, namely, the width and length of the small orifice. To examine the effects experimentally, three small orifices of different sizes, 0.51 μm in width and 15 μm in length, 1.5 μm in width and 15 μm in length, and 1.5 μm in width and 5 μm in length, were tested for separating 1 and 3 micron particles. In all these tests, the width of the large orifice is fixed at 125 μm.

Figure 8a shows the particle separation with a small orifice of 1.5 μm in width and 15 μm in length. In this case, the 1 μm and 3 μm particles are separated clearly under 140 volts. When the width of the small orifice is reduced from 1.5 μm to 510 nm, the width ratio between the small orifice and the large orifice is increased by 3 times, hence the electric field gradient is significantly increased. While, similar to the cases shown in Figure 3a and Figure 3b, the area of high $\nabla|E|^2$ (high DEP force area) outside the small orifice becomes smaller with the decrease of the small orifice width, weakening the DEP separation. To achieve the same separation effect, a higher electric potential has to be applied so that the area of high $\nabla|E|^2$ outside the small orifice can be larger when the width of the small orifice is smaller. Figure 8b shows particles separation with a small orifice of 0.51 μm in width and 15 μm in length. In comparison with the case of Figure 8a, the width of the small orifice is smaller in this case (Figure 8b), the 1 μm and 3 μm particles are separated clearly under a higher voltage 340 volts.

When the length of the small orifice is reduced, the electric resistance of the small orifice is reduced and hence the electric potential drop inside the small orifice is reduced. Correspondingly, the area of high $\nabla|E|^2$ (high DEP force area) outside the small orifice becomes larger, under a given applied voltage, as shown in Figure 3b and Figure 3c. In other words, to achieve the same DEP separation effect, the applied voltage can be smaller when the length of the small orifice is smaller. Figures 8a and 8c demonstrate that the separation of the 1 μm and 3 μm particles can be realized with a significantly reduced voltage of 30 V (from 140 V) when the length of the small orifice is reduced from 15 μm to 5 μm. In summary, greater DEP force can be generated by using a large orifice width ratio and a small orifice of short length at low voltages.

Separation of nanoparticles

In order to examine the sensitivity of this proposed separation method, the DC-DEP separation experiments with mixtures of 140 nm particles and 500 nm particles, and mixtures of 51 nm

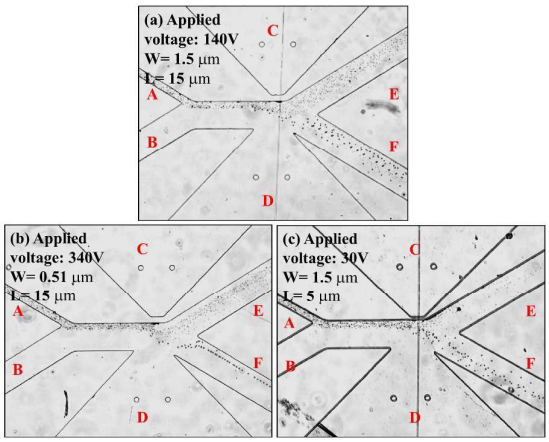

Figure 8. Effects of the width and length of the small orifice on DEP separation of particles in terms of the applied voltage. Differences between (a) and (b): The small orifice width is reduced from 1.5 μm to 0.51 μm, and the applied voltage is increased from 140 V to 340 V. Differences between (a) and (c): The small orifice length is reduced from 15 μm to 5 μm, and the applied voltage is reduced from 140 V to 30 V.

View Article Online
DOI: 10.1039/C6NR06952E

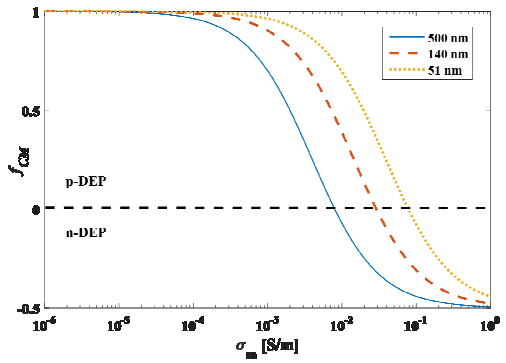

Figure 9. Prediction of f_{CM} for three different sizes of polystyrene particles as a function of the electric conductivity of the suspending solution σ_m. 0

particles and 140 nm particles were conducted. As the particle size decreases from micron to nanometer, the DEP force exerted on the nanoparticles is dramatically reduced and hence the separation of nanoparticles by size with the same type of DEP force (i.e., negative DEP force) becomes difficult. Therefore, we propose to separate the nanoparticles by adjusting the electrical conductivity of the suspending solution, so that the nanoparticles of a given size experience positive DEP force while the nanoparticles of another size experience negative DEP. Consequently, the nanoparticles with different DEP behaviors can be continuously separated.

The DEP behaviors of the particles are determined by the Clausius-Mossotti factor (f_{CM}) which represents the relative polarizability of the particles with respect to the surrounding

solution. Under DC electric fields, the f_{CM} can be expressed as [57,58]

$$f_{CM} = \left(\frac{\sigma_p - \sigma_m}{\sigma_p + 2\sigma_m}\right) \qquad \text{Eq. (3)}$$

where σ_p and σ_m are the electrical conductivity of the particle and suspending solution, respectively.
The conductivity of polystyrene particles can be estimated by [59,60]

$$\sigma_p = \sigma_b + \frac{2K_s}{r} \qquad \text{Eq. (4)}$$

where σ_b is the bulk conductivity of particle and can be considered negligible for polystyrene particles, and K_s is the surface conductance (typically $K_s = 1\ nS$ for polystyrene), and *r* is the radius of the particle.

In Figure 9, f_{CM} values of the nanoparticles of three different sizes, 51 nm, 140 nm and 500 nm are plotted as a function of the electric conductivity of the suspending solution, σ_m. It can be seen that f_{CM} value ranges from −0.5 to 1, and. In a certain range of σ_m, $f_{\mathrm{CM}} > 0$ (i.e., positive DEP force) for nanoparticles of a given size, while $f_{\mathrm{CM}} < 0$ (i.e., negative DEP force) for nanoparticles of another size. In this study, two suspending solutions with two different conductivities were used, 0.4 mM K_2HPO_4 solution with a pH 7 and a conductivity of 1×10^{-2} S/m was used for the separation of 140 nm and 500 nm particles, and 1.6 mM K_2HPO_4 solution with a pH 7 and a conductivity of 4×10^{-2} S/m was employed for the separation of 51 nm and 140 nm particles. The corresponding f_{CM} values are listed in Table 2.

Generally, the electrical force on a spherical particle is expressed as [1]

$$\mathrm{F_e} = 4\pi\varepsilon_m\,\zeta_p\,r\,(1+\kappa r)E \qquad \text{Eq. (5)}$$

where ζ_p is the zeta potential of particles, and $1/\kappa$ is the characteristic thickness of electrical double layer (EDL). The particles used in this work are all negatively charged and their electrophoretic motion directs to the positive electrode. The force ratio between electrical force and DEP force is given by

$$\frac{\mathrm{F_e}}{\mathrm{F_{DEP}}} = \frac{2\,\zeta_p\,(1+\kappa r)E}{r^2\,\mathrm{Re}(f_{\mathrm{CM}})(\nabla|E|^2)} \approx \frac{2\,\zeta_p\,\kappa\,E}{r\,\mathrm{Re}(f_{\mathrm{CM}})\,(\nabla|E|^2)} \quad (\text{for thin EDL}) \qquad \text{Eq. (6)}$$

The ratio between the electrical force and DEP force on the particle is increased by 10^3 when the size of the particle decreases from micron scale to the nanoscale. This indicates the electrophoretic motion of nanoparticles is important and can be favorable for DEP separation of nanoparticles by adjusting the position of the positive electrode (i.e., the polarity of the applied electric field). In the DC-DEP separation of nanoparticles, the electrical conductivity of the suspending medium was selected in such a way that the nanoparticles of a given size experience positive DEP force (attracting to the strong electric field at the small orifice) while the nanoparticles of another size experience negative DEP (being repelled away from the small orifice). Therefore, in these experiments, electrode D (on the opposite side to the small orifice) was selected as the positive electrode. In this way, the electrophoresis motion of the nanoparticles is in the same direction as the negative DEP, enhancing the separation of the particles undergoing negative DEP.

Based on the calculated f_{CM} in Table 2, the numerical simulation of the trajectory of 140 nm and 500 nm particles has been conducted by COMSOL 4.3b via the particle tracing

Table 2. The Clausuis-Mossotti factor (f_{CM}) for the polystyrene particles of three different sizes in the suspending medium with two different electric conductivities.

Diameter of particle (nm)	f_{CM} with σ_m = 1 × 10^{-2} S/m, 0.4 mM K_2HPO_4 solution	f_{CM} with σ_m = 4 × 10^{-2} S/m, 1.6 mM K_2HPO_4 solution
500	−0.07	
140	0.38	−0.1
51		0.24

View Article Online
DOI: 10.1039/C6NR06952E

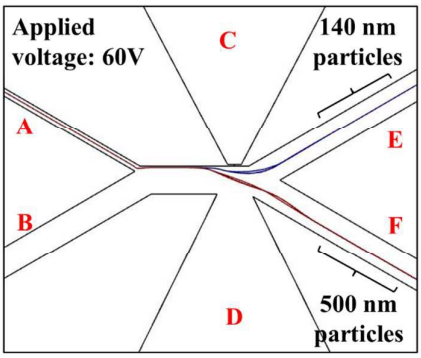

Figure 10. Numerical simulation of the separation of the 140 nm and 500 nm particles. 60 V is applied at electrode D, and zero volt is applied at electrode C. The width and length of the small orifice are 0.51 μm and 5 μm, respectively, and the large orifice width is 125 μm.

module. Figure 10 shows the separation of 140 nm and 500 nm particles with 60 V applied at electrode D. The width and length of the small orifice are 0.51 μm and 5 μm, respectively, and the large orifice width is 125 μm.

By using a selected suspending medium, the separation based on the opposite dielectrophoretic behaviors as a function of particle sizes is shown in Figures 11 and 12. It should be noted that the conventional non-fluorescent microscope cannot see any particles smaller than 200~300 nm. In these experiments, therefore, 51 nm and 140 nm fluorescent particles were used in order to show their trajectories. The 500 nm particles used in the experiments are non-fluorescent particles. Figure 11a and Figure 11b shows that the mixture of 140 nm and 500 nm particles was well separated by inducing positive DEP force on 140 nm particles which were attracted to the small orifice area and moved into outlet channel E, and by inducing negative DEP force on the 500 nm particles which were repelled from the small orifice and moved to the outlet channel F. In Figure 12a and Figure 12b, the fluorescent images clearly show the separated trajectories of the red fluorescent 51 nm particles and green fluorescent 140 nm particles. Evidently, the mixed red fluorescent 51 nm particles and green fluorescent 140 nm particles were separated and directed into outlet channels E and F by positive-DEP and negative-DEP, respectively. This indicates that the proposed nano-orifice based DC-DEP separation method can be used for the separation of nanoparticles with smaller size differences, i.e., a 90 nm size difference as demonstrated in Figure 12.

Conclusions

A novel nano-orifice based DC-DEP method for continuous separation of polystyrene microparticles and nanoparticles by size in a pressure-driven flow is developed. The motion of particles is controlled by the pressure-driven flow, and a local DC electric field is employed to induce a non-uniform electric field via a pair of asymmetric orifices on the opposite channel walls. The particles mixture experiences DEP force when passing through the vicinity of the small orifice where exits the strongest electric field gradient and the mixed particles are separated into two different streams and moved into two individual outlet channels. Effects of key parameters such as electric field, and the width and length of the small orifice were investigated experimentally in this study. Using a larger orifice width ratio and a shorter small orifice can generate a strong gradient of the non-uniform electric field and hence strong DEP force under a lower applied voltage. By adjusting the applied electrical voltage and the electrical conductivity of the suspending solution, this new method can separate nanoparticles as small as 51 nm and 140 nm in diameter, i.e. with a size difference of 90 nm. The major advantages of this DC-DEP separation method include: (1) The fabrication process of the microfluidic chip is simple; (2) The asymmetric orifices

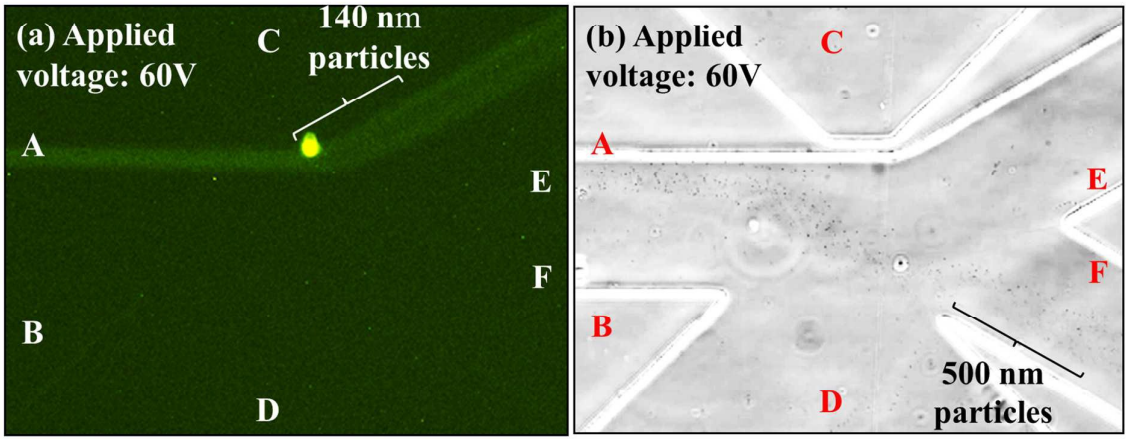

Figure 11. Separation of 140 nm and 500 nm particles. (a) Fluorescent image showing the trajectories of 140 nm fluorescent (green) particles. (b) Trajectories of 500 nm non-fluorescent particles. 60 V is applied at electrode D. The width and length of the small orifice are 0.51 μm and 5 μm, respectively, and the large orifice width is 125 μm.

View Article Online
DOI: 10.1039/C6NR06952E

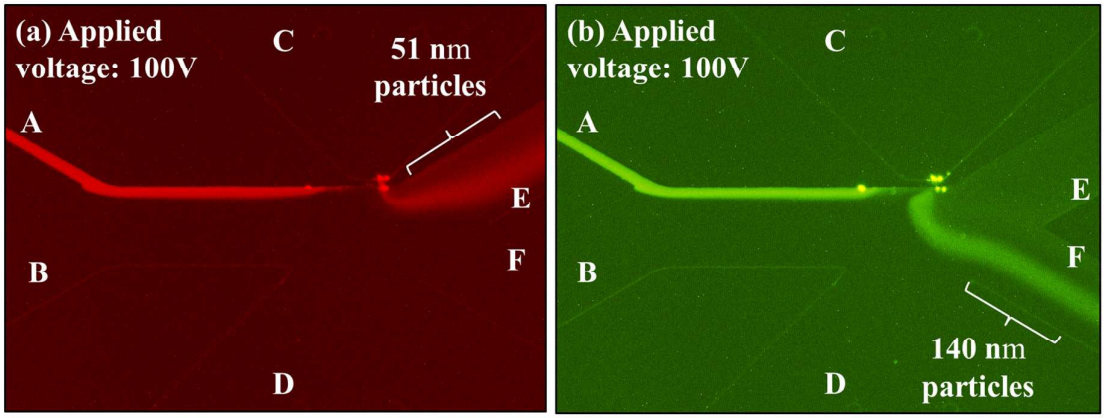

Figure 12. Separation of 51 nm and 140 nm particles. (a) Fluorescent image showing the trajectories of 51 nm particles. (b) Fluorescent image showing the trajectories of 140 nm particles. 100 V is applied at electrode D. The width and length of the small orifice are 0.51 μm and 5 μm, respectively, and the large orifice width is 125 μm.

structure enables to generate a strong electric field gradient, which allows the separation of particles with smaller size differences and separation of nanoparticles; (3) There is no high electric field applied through the whole microchannel, and the Joule heating effect is essentially avoided; (4) The generation of the local electrical field gradient does not require the change of the cross section of the microchannel and will not affect the transport of the particles.

Acknowledgements

The authors wish to thank the Natural Sciences and Engineering Research Council (NSERC) of Canada for financial support through a research grant to Dr. Li.

References

1 Dongqing Li, *Electrokinetics in Microfluidics*, 2004.
2 Y. C. Lim, A. Z. Kouzani and W. Duan, *Microsyst. Technol.*, 2010, **16**, 1995–2015.
3 A. Arora, G. Simone, G. B. Salieb-Beugelaar, J. T. Kim and A. Manz, *Anal. Chem.*, 2010, **82**, 4830–4847.
4 S. Haeberle, D. Mark, F. Von Stetten and R. Zengerle, *Microsystems Nanotechnol.*, 2012, 853–895.
5 H. Andersson and A. Van den Berg, *Sensors Actuators, B Chem.*, 2003, **92**, 315–325.
6 and F. F. B. Holzel, R., *IEE Proceedings-Nanobiotechnology*, 2003, **150**, 47–53.
7 P. R. C. Gascoyne and J. Vykoukal, *Electrophoresis*, 2002, **23**, 1973.
8 M. P. Hughes, *Electrophoresis*, 2002, **23**, 2569–2582.
9 K. H. Kang, Y. Kang, X. Xuan and D. Li, *Electrophoresis*, 2006, **27**, 694–702.
10 I. Barbulovic-Nad, X. Xuan, J. S. H. Lee and D. Li, *Lab Chip*, 2006, **6**, 274–279.
11 C. Zhang, K. Khoshmanesh, A. Mitchell and K. Kalantar-Zadeh, *Anal. Bioanal. Chem.*, 2010, **396**, 401–420.
12 D. Chen, H. Du and C. Y. Tay, *Nanoscale Res. Lett.*, 2010, **5**, 55–60.
13 R. Krishnan, B. D. Sullivan, R. L. Mifflin, S. C. Esener and M. J. Heller, *Electrophoresis*, 2008, **29**, 1765–1774.
14 D. H. Shin, J. E. Kim, H. C. Shim, J. W. Song, J. H. Yoon, J. Kim, S. Jeong, J. Kang, S. Baik and C. S. Han, *Nano Lett.*, 2008, **8**, 4380–4385.
15 C. Zhang, K. Khoshmanesh, F. Tovar-Lopez, A. Mitchell, W. Wlodarski and K. Klantar-zadeh, *Microfluid. Nanofluidics*, 2009, **7**, 633–645.
16 B. H. Lapizco-Encinas, B. A. Simmons, E. B. Cummings and Y. Fintschenko, *Anal. Chem.*, 2004, **76**, 1571–1579.
17 Y. Huang, J. M. Yang, P. J. Hopkins, S. Kassegne, M. Tirado, A. H. Forster and H. Reese, *Biomed. Microdevices*, 2003, **5**, 217–225.
18 B. H. Lapizco-Encinas, R. V. Davalos, B. a. Simmons, E. B. Cummings and Y. Fintschenko, *J. Microbiol. Methods*, 2005, **62**, 317–326.
19 B. H. Lapizco-Encinas, S. Ozuna-Chacón and M. Rito-Palomares, *J. Chromatogr. A*, 2008, **1206**, 45–51.
20 L. Zheng, J. P. Brody and P. J. Burke, *Biosens. Bioelectron.*, 2004, **20**, 606–619.
21 M. Washizu, *J. Electrostat.*, 2005, **63**, 795–802.
22 A. I. K. Lao and I.-M. Hsing, *Lab Chip*, 2005, **5**, 687–90.
23 F. Grom, J. Kentsch, T. Müller, T. Schnelle and M. Stelzle, *Electrophoresis*, 2006, **27**, 1386–1393.
24 I. Ermolina, H. Morgan, N. G. Green, J. J. Milner and Y. Feldman, *Biochim. Biophys. Acta - Gen. Subj.*, 2003, **1622**, 57–63.
25 I. Oita, H. Halewyck, B. Thys, B. Rombaut, Y. Vander Heyden and D. Mangelings, *Anal. Bioanal. Chem.*, 2010, **398**, 239–264.
26 Y. Kang, D. Li, S. a. Kalams and J. E. Eid, *Biomed. Microdevices*, 2008, **10**, 243–249.
27 Z. R. Gagnon, *Electrophoresis*, 2011, **32**, 2466–2487.
28 J. Voldman, *Annu. Rev. Biomed. Eng.*, 2006, **8**, 425–454.
29 Y. Kang and D. Li, *Microfluid. Nanofluidics*, 2009, **6**, 431–460.
30 D. R. Gossett, W. M. Weaver, A. J. MacH, S. C. Hur, H. T. K.

View Article Online
DOI: 10.1039/C6NR06952E

Tse, W. Lee, H. Amini and D. Di Carlo, *Anal. Bioanal. Chem.*, 2010, **397**, 3249–3267.
31 R. Carlson, C. Gabel, S. Chan, R. Austin, J. Brody and J. Winkelman, *Phys. Rev. Lett.*, 1997, **79**, 2149.
32 D. G. Grier, *Nature*, 2003, **424**, 810–6.
33 K. E. Mccloskey, J. J. Chalmers and M. Zborowski, *Anal. Chem.*, 2003, **75**, 6868–6874.
34 A. Ramos, H. Morgan, N. G. Green and A. Castellanos, *J. Electrostat.*, 1999, **47**, 71–81.
35 D. Juncker, H. Schmid and E. Delamarche, *Nat. Mater.*, 2005, **4**, 622–628.
36 A. Nilsson, F. Petersson, H. Jönsson and T. Laurell, *Lab Chip*, 2004, **4**, 131–135.
37 F. Petersson, A. Nilsson, C. Holm, H. Jonsson and T. Laurell, *Lab Chip*, 2005, **5**, 20–2.
38 R. Cezar de Andrade Costa, K. B. Mogensen and J. P. Kutter, *Lab Chip*, 2005, **5**, 1310–4.
39 B. Çetin and D. Li, *Electrophoresis*, 2011, **32**, 2410–2427.
40 K. Khoshmanesh, S. Nahavandi, S. Baratchi, A. Mitchell and K. Kalantar-zadeh, *Biosens. Bioelectron.*, 2011, **26**, 1800–1814.
41 P. R. C. Gascoyne, Y. Huang, R. Pethig, J. Vykoukal and F. F. Becker, *Meas. Sci. Technol.*, 1999, **3**, 439–445.
42 K. Khoshmanesh, C. Zhang, J. L. Campbell, A. A. Kayani, S. Nahavandi, A. Mitchell and K. Kalantar-Zadeh, *Microfluid. Nanofluidics*, 2010, **9**, 755–763.
43 C. Yu, J. Vykoukal, D. M. Vykoukal, J. a. Schwartz, L. Shi and P. R. C. Gascoyne, *J. Microelectromechanical Syst.*, 2005, **14**, 480–487.
44 R. C. Gallo-Villanueva, C. E. Rodríguez-López, R. I. Díaz-de-la-Garza, C. Reyes-Betanzo and B. H. Lapizco-Encinas, *Electrophoresis*, 2009, **30**, 4195–4205.
45 A. Gencoglu and A. Minerick, *Lab Chip*, 2009, **9**, 1866–1873.
46 E. B. Cummings and A. K. Singh, *Anal. Chem.*, 2003, **75**, 4724–4731.
47 B. H. Lapizco-Encinas, B. A. Simmons, E. B. Cummings and Y. Fintschenko, *Electrophoresis*, 2004, **25**, 1695–1704.
48 B. Cetin and D. Li, *Electrophoresis*, 2008, **29**, 994–1005.
49 T B Jones, *Electromechanics of particles*, Cambridge University Press, 1995.
50 R. Peng and D. Li, *Biomicrofluidics*, 2015, **9**, 024117.
51 K. M. Choi and J. A. Rogers, *J. Am. Chem. Soc.*, 2003, **125**, 4060–4061.
52 D. C. Duffy, J. C. McDonald, O. J. A. Schueller and G. M. Whitesides, *Anal. Chem.*, 1998, **70**, 4974–4984.
53 J. Zhu, R. C. Canter, G. Keten, P. Vedantam, T. R. J. Tzeng and X. Xuan, *Microfluid. Nanofluidics*, 2011, **11**, 743–752.
54 M. Li, S. Li, W. Li, W. Wen and G. Alici, *Electrophoresis*, 2013, **34**, 952–960.
55 C. Church, J. Zhu and X. Xuan, *Electrophoresis*, 2011, **32**, 527–531.
56 J. Sun, Y. Gao, R. J. Isaacs, K. C. Boelte, P. Charles Lin, E. M. Boczko and D. Li, *Anal. Chem.*, 2012, **84**, 2017–2024.
57 G. H. Markx, P. A. Dyda and R. Pethig, *J. Biotechnol.*, 1996, **51**, 175–180.
58 Dongqing Li, *Encyclopedia of Microfluidics and Nanofluidics*, 2008, vol. 1.
59 I. Ermolina and H. Morgan, *J. Colloid Interface Sci.*, 2005, **285**, 419–428.
60 C. T. O'Konski, *J. Phys. Chem.*, 1960, **64**, 605–619.